

A Giant Metrewave Radio Telescope search for associated HI 21 cm absorption in high-redshift flat-spectrum sources

J. N. H. S. Aditya^{*}, Nissim Kanekar[†], Sushma Kurapati

National Centre for Radio Astrophysics, Tata Institute of Fundamental Research, Pune 411007, India

9 April 2018

ABSTRACT

We report results from a Giant Metrewave Radio Telescope search for “associated” redshifted HI 21 cm absorption from 24 active galactic nuclei (AGNs), at $1.1 < z < 3.6$, selected from the Caltech-Jodrell Bank Flat-spectrum (CJF) sample. 22 out of 23 sources with usable data showed no evidence of absorption, with typical 3σ optical depth detection limits of ≈ 0.01 at a velocity resolution of $\approx 30 \text{ km s}^{-1}$. A single tentative absorption detection was obtained at $z \approx 3.530$ towards TXS 0604+728. If confirmed, this would be the highest redshift at which HI 21 cm absorption has ever been detected.

Including 29 CJF sources with searches for redshifted HI 21 cm absorption in the literature, mostly at $z < 1$, we construct a sample of 52 uniformly-selected flat-spectrum sources. A Peto-Prentice two-sample test for censored data finds (at $\approx 3\sigma$ significance) that the strength of HI 21 cm absorption is weaker in the high- z sample than in the low- z sample; this is the first statistically significant evidence for redshift evolution in the strength of HI 21 cm absorption in a uniformly selected AGN sample. However, the two-sample test also finds that the HI 21 cm absorption strength is higher in AGNs with low ultraviolet or radio luminosities, at $\approx 3.4\sigma$ significance. The fact that the higher-luminosity AGNs of the sample typically lie at high redshifts implies that it is currently not possible to break the degeneracy between AGN luminosity and redshift evolution as the primary cause of the low HI 21 cm opacities in high-redshift, high-luminosity active galactic nuclei.

Key words: galaxies: active — quasars: absorption lines — galaxies: high redshift — radio lines: galaxies

1 INTRODUCTION

The generally accepted model of an active galactic nucleus (AGN) consists of a central super-massive black hole surrounded by an accretion disk and clouds of ionized, atomic and molecular gas. The energy output from the AGN is thought to be fuelled by the supply of gas onto the central black hole (e.g. Rees 1984). The gas may be supplied to the central regions either through slow accretion of material from larger scales, or through the triggering of gas infall by galaxy mergers (e.g. Struve et al. 2010). Conversely, the AGN also may give rise to energetic gas outflows, resulting in the quenching of star formation in the central regions, and possibly even ending the active state of the nucleus (e.g. Fabian 2012). Studies of the distribution and kinematics of the circumnuclear gas allow us to probe the relative importance of infall and outflows at different redshifts, yielding insights into the fuelling of AGN activity and feedback mechanisms, both of which have strong influence on galaxy evolution.

In the case of radio-loud AGNs, absorption studies in the HI 21 cm line provide an interesting probe of gas kinematics in the nuclear regions (see, e.g., Morganti 2012, for a recent review). Such “associated” HI 21 cm absorption studies can be used to test AGN unification schemes (e.g. Barthel 1989). These scenarios predict that the line of sight to broad-line AGNs is normal to the torus (and to the thick disk), while that toward narrow-line AGNs lies close to the plane of the torus. Unification schemes hence suggest that associated HI 21 cm absorption should be systematically more common in the latter class of systems, as the nucleus in broad-line systems is not expected to be obscured by the neutral gas. Associated HI 21 cm absorption studies can also be used to identify and study circumnuclear disks and tori around AGNs (e.g. Conway & Blanco 1995; Carilli et al. 1998; Peck & Taylor 2002; Morganti et al. 2008). Finally, associated absorbers with high HI column densities are also likely to show molecular absorption in transitions of species like CO, HCO^+ , OH, etc. (e.g. Carilli et al. 1992; Carilli et al. 1997; Wiklind & Combes 1994; Wiklind & Combes 1996; Kanekar & Chengalur 2002, 2008). Such systems allow further detailed studies of physical and chemical properties of the AGN environment. In addition, comparisons between the redshifts of different atomic and molecular transitions in such systems allow

^{*} E-mail: aditya@ncra.tifr.res.in (JNHSA); nkanekar@ncra.tifr.res.in (NK); sushma@ncra.tifr.res.in (SK)

[†] Swarnajayanti Fellow

one to probe the possibility of changes in the fundamental constants of physics, such as the fine structure constant and the proton-electron mass ratio (e.g. Drinkwater et al. 1998; Carilli et al. 2000; Chengalur & Kanekar 2003; Kanekar et al. 2004, 2010).

While searches for associated HI 21 cm absorption have been carried out for about three decades, conditions in the neutral gas in AGN environments are still unclear. The first such study was that of van Gorkom et al. (1989) who used the Very Large Array to search for HI 21 cm absorption in a well-defined sample of nearby radio galaxies. They found that the detected HI 21 cm absorption features tend to be redshifted from the systemic velocity of the targets, i.e. that gas infall appears to be more common than gas outflow in local AGNs. Interestingly, their estimated mass supply rate from the gas velocities was much larger than required to fuel the AGN radio activity (only $\approx 10^{-5} - 10^{-3} M_{\odot} \text{ yr}^{-1}$), indicating that cold atomic gas might be the main fuel source for this activity. Later, however, Vermeulen et al. (2003) used the Westerbork Synthesis Radio Telescope to search for associated HI 21 cm absorption in a large, heterogeneous AGN sample at intermediate redshifts ($0.2 \lesssim z \lesssim 0.8$) and found comparable numbers of redshifted and blueshifted absorption features (see also Pihlström et al. 2003). Their results indicate that both infall and outflow may be important in AGN environments, with the complex absorption profiles possibly arising from interactions of the neutral gas with the radio jets or gas rotation around the central nucleus. Later searches for HI 21 cm absorption in large, but again heterogeneous, samples (e.g. Gupta et al. 2006; Curran et al. 2008; Geréb et al. 2015) have been unable to shed much light on whether or not the inflow of neutral gas is likely to be the main source of AGN fuel. We note, in passing, that a strong correlation has recently been found between the accretion rates of hot X-ray emitting gas, associated with the hot corona, and the AGN jet power (e.g. Allen et al. 2006). These results suggest that hot X-ray emitting gas could be an important component of the fuel that powers the active nucleus.

The above studies of associated HI 21 cm absorbers have found absorption features having a wide range of line profiles (e.g. both narrow and broad), and differing offsets from the systemic velocity, indicating complex morphologies of the gaseous structures around the central core (e.g. Gupta et al. 2006; Geréb et al. 2015). Narrow lines with smaller velocity offsets ($\leq 100 \text{ km s}^{-1}$) from the AGN redshift would indicate gas clouds with small velocity dispersions, possibly rotating in circumnuclear disks, whereas broader absorption features suggest unsettled gas, perhaps interacting with the central radio source. Features with the largest widths ($\gtrsim 200 \text{ km s}^{-1}$) are likely to arise due to interactions between the gas and the AGN radio jet. These wide and typically blueshifted absorption features are more commonly found in compact sources (e.g. Pihlström et al. 2003; Gupta et al. 2006; Geréb et al. 2015), indicating that such sources may be the best targets for searches for radio source-gas interactions as well as strong AGN-driven outflows. The outflowing gas is expected to be deposited in the intergalactic medium (IGM), transferring energy back to the IGM, and thus regulating gas collapse and hence star formation in the AGN host galaxy via feedback. Such feedback mechanisms have been shown to be critical in understanding galaxy formation: specifically, simulations of galaxy evolution which do not implement feedback models produce far higher star formation rates (SFRs) than the typical SFRs observed in the Universe, while those that include some prescription for feedback tend to be consistent with the observed data (e.g. Springel et al. 2005). Despite its acknowledged importance, our understanding of feedback effects in galaxies is very limited, and it is as yet even unclear which of the

two most prominent feedback mechanisms, AGN-induced feedback (e.g. Fabian 2012; Morganti et al. 2013) and supernovae outbursts (e.g. Efsthathiou 2000), is the dominant process for the regulation of star formation. The detection of blueshifted absorption features is a signature of gas outflows and can thus be used to trace the importance of feedback at different redshifts, and in different AGN types. Follow-up Very Long Baseline Interferometry (VLBI) mapping studies in the redshifted HI 21 cm line can then be possibly used to trace the location of the gas outflows and determine whether they arise from the AGN or from supernovae (e.g. Morganti et al. 2013).

HI 21 cm absorption studies thus provide an important probe of the distribution and kinematics of neutral hydrogen gas in AGN environments, and their redshift evolution (e.g. Kanekar & Briggs 2004). Unfortunately, previous surveys for associated HI 21 cm absorption have been mostly limited to low redshifts ($z \leq 1$) (e.g. Morganti et al. 2001; Vermeulen et al. 2003; Gupta et al. 2006), with only a handful of such searches at $z > 1$ in the literature (e.g. Gupta et al. 2006; Curran et al. 2013), some of which have low sensitivity. Indeed, there are currently only four detections of associated HI 21 cm absorbers at $z \geq 1$, at $z \approx 1.2$ towards 3C190 (Ishwara-Chandra et al. 2003), $z \approx 1.3$ towards J1545+4751 (Curran et al. 2013), $z \approx 2.6$ towards MG J0414+0534 (Moore et al. 1999), and $z \approx 3.4$ towards TXS 0902+343 (Uson et al. 1991).

The main hindrance to using HI 21 cm absorption studies to probe the redshift evolution of AGN environments is the paucity of HI 21 cm absorbers at high redshifts, $z > 1$. Further, most studies in the literature at higher redshifts (e.g. Gupta et al. 2006; Curran et al. 2013) have targeted heterogeneous samples for which it is often difficult to separate redshift effects from source characteristics. We have hence begun a project to use the Giant Metrewave Radio Telescope (GMRT) to carry out a search for associated HI 21 cm absorption in a large sample of high- z flat spectrum sources, selected in a uniform manner. In this paper, we present initial results from this project, from a GMRT search for redshifted HI 21 cm absorption in 24 AGNs of the sample, at $z \approx 1.3$ and $z \approx 3.5$.

2 THE SAMPLE, OBSERVATIONS, DATA ANALYSIS AND RESULTS

2.1 The Caltech-Jodrell Bank flat-spectrum sample

A number of studies, mostly targeting AGNs at low redshifts, $z \lesssim 1$, have established that the integrated HI 21 cm optical depth is inversely correlated with the spatial extent of the radio emission (e.g. Pihlström et al. 2003; Gupta et al. 2006). For example, Gupta et al. (2006) found that the detection rate of HI 21 cm absorption in their sample of 96 sources was highest for the most compact, gigahertz-peaked-spectrum (GPS) sources, and lowest for steep-spectrum sources with extended radio continua. We hence used source compactness as the primary criterion in selecting our target AGN sample. Further, both inverted-spectrum (e.g. GPS) and flat-spectrum AGNs are expected to be relatively compact, as the flattening of the radio spectrum at low frequencies is believed to arise from synchrotron self-absorption (e.g. O’Dea 1998). We hence decided to target flat-spectrum sources as these provide a balance between compactness and sufficient low-frequency flux density for deep searches for redshifted HI 21 cm absorption.

The Caltech-Jodrell Bank flat-spectrum (CJF) sample

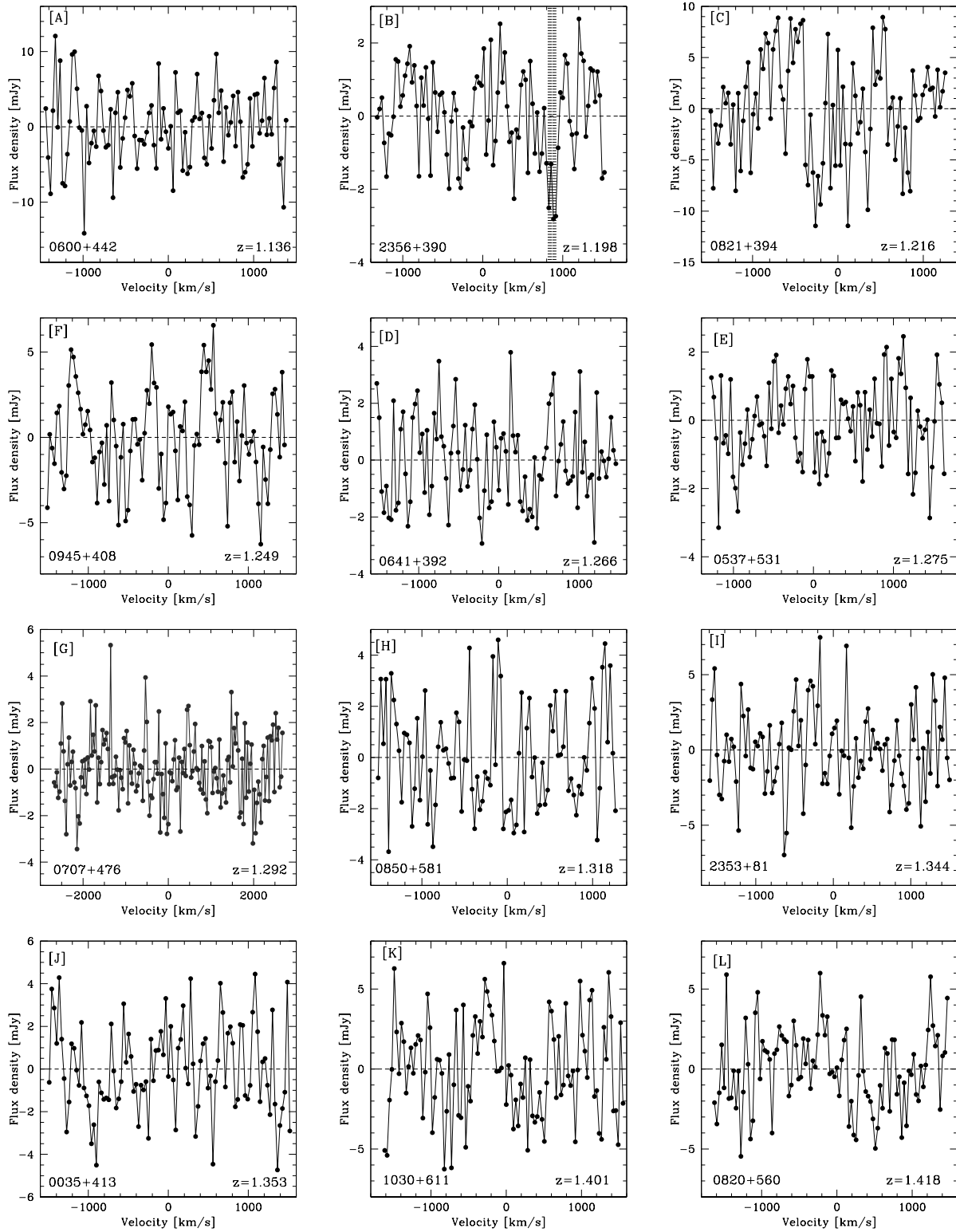


Figure 1. The GMRT HI 21 cm spectra for the 23 sources with usable data; all spectra have been Hanning-smoothed and re-sampled. The shaded channels in the spectrum of the source TXS 2356+390 are corrupted by RFI.

Table 1. The 24 targets of this paper, selected from the CJF sample, in order of increasing redshift. Note that $L'_{UV} = \text{Log}[L_{UV}/W \text{ Hz}^{-1}]$ and $L'_{1.4 \text{ GHz}} = \text{Log}[L_{1.4 \text{ GHz}}/W \text{ Hz}^{-1}]$.

Source	z	$\nu_{21 \text{ cm}}$ MHz	BW MHz	Δv km s^{-1}	S_ν mJy	ΔS mJy	$\int \tau dV$ km s^{-1}	L'_{UV}	$L'_{1.4 \text{ GHz}}$	$\alpha_{21 \text{ cm}}$
TXS 0600+442	1.136	664.98	8.0	28.2	1260.7 ± 0.6	4.9	< 0.71	—	27.61	-0.37
TXS 2356+390	1.198	646.23	8.0 ^b	29.0	643.0 ± 0.5	1.2	< 0.42	22.36	27.36	-1.16
TXS 0821+394	1.216	641.08	8.0	29.2	2532.8 ± 0.4	5.1	< 0.44	23.56	27.97	-0.75
TXS 0945+408	1.249	631.56	8.0	29.7	2026.0 ± 0.5	2.8	< 0.30	23.93	27.89	-0.46
TXS 0641+392	1.266	626.83	8.0	29.9	417.7 ± 0.3	1.5	< 0.68	22.04	27.22	0.79
TXS 0537+531	1.275	624.35	8.0	30.0	711.3 ± 0.5	1.2	< 0.32	22.85	27.46	0.01
TXS 0707+476	1.292	619.72	33.3	31.5 ^a	1022.5 ± 0.2	1.4	< 0.30	23.86	27.63	-0.15
TXS 0850+581	1.318	612.89	8.0	30.6	998.6 ± 0.5	2.0	< 0.37	23.53	27.63	-0.26
S5 2353+81	1.344	605.98	8.0	30.9	581.6 ± 0.6	2.7	< 0.87	22.31	27.41	-0.53
TXS 0035+413	1.353	603.66	8.0	31.0	541.8 ± 0.6	2.1	< 0.76	23.12	27.39	0.35
TXS 1030+611	1.401	591.60	8.0	31.7	692.1 ± 0.5	3.1	< 0.87	23.57	27.53	-0.37
TXS 0820+560	1.418	587.34	8.0	31.9	1507.7 ± 0.1	2.5	< 0.34	23.69	27.87	-0.26
TXS 0805+410	1.418	587.32	8.0	31.9	512.3 ± 0.8	2.0	< 0.69	23.32	27.40	-0.07
TXS 0804+499	1.436	583.08	8.0	32.1	682.6 ± 0.5	3.6	< 0.95	23.45	27.54	0.31
TXS 0917+624	1.446	580.71	8.0	32.3	975.6 ± 0.5	4.2	< 0.79	23.22	27.70	0.23
TXS 0859+470	1.470	575.05	8.0	32.6	2819.5 ± 0.4	6.2	< 0.43	23.68	28.17	-0.23
TXS 2253+417	1.476	573.67	8.0	32.6	1255.2 ± 0.5	4.5	< 0.71	—	27.82	0.30
TXS 0340+362	1.484	571.82	8.0	33.0	291.4 ± 0.5	4.7	< 3.00	21.85	27.19	0.35
TXS 0800+618	3.033	352.20	4.0	26.6	858.5 ± 0.5	6.7	< 1.17	23.67	28.22	-0.05
S5 0014+81	3.366	325.33	4.0 ^b	28.8	773.5 ± 0.4	RFI	RFI	25.25	28.27	-0.11
TXS 0642+449	3.396	323.11	4.0	29.0	310.6 ± 1.1	4.2	< 2.86	24.48	27.86	0.72
TXS 0620+389	3.469	317.84	4.0	29.5	1608.3 ± 0.8	8.3	< 0.20	23.95	28.50	-0.16
TXS 0604+728	3.530	313.56	4.0	29.9	1890.9 ± 1.9	3.5	4.29 ± 0.28	23.63	28.64	-0.38
TXS 0749+426	3.589	309.51	4.0	30.3	537.5 ± 0.6	2.0	< 0.76	24.61	28.14	0.16

^aIn the case of TXS 0707+476, the listed velocity resolution in Column (5) is without Hanning-smoothing and re-sampling.

^bThe listed bandwidths and resolutions for TXS 2356+390 and S5 0014+81 are for the original observations with the hardware backend. Both sources were re-observed using the software backend, with 512 channels; the bandwidth and velocity resolution were 33.3 MHz and $\approx 30.2 \text{ km s}^{-1}$ for TXS 2356+390, and 16.7 MHz and $\approx 30.0 \text{ km s}^{-1}$ for S5 0014+81 (for both sources, the quoted resolutions are without Hanning-smoothing and re-sampling).

(Pearson & Readhead 1988; Polatidis et al. 1995; Henstock et al. 1995; Taylor et al. 1996) was used to select our target AGNs, for the following reasons: (1) the flat-spectrum criterion implies that the sources of the CJF sample are extremely compact, (2) accurate redshifts are available for most of the CJF sample, from follow-up optical spectroscopy (e.g. Henstock et al. 1997), (3) the CJF sources are all relatively bright at radio frequencies, with 5 GHz flux densities $> 350 \text{ mJy}$ (e.g. Taylor et al. 1996), (4) VLBI information is available for all CJF sources, at frequencies of $\approx 1-5 \text{ GHz}$, providing additional details of their spatial structure (e.g. Polatidis et al. 1995; Taylor et al. 1996), and (5) low-frequency flux density estimates are available for all CJF sources from the 325 MHz Westerbork Northern Sky Survey (WENSS) (Rengelink et al. 1997) or the 365 MHz Texas survey (Douglas et al. 1996).

For the pilot GMRT HI 21 cm absorption survey reported here, we chose to focus on the brightest CJF sources, and hence imposed the additional criterion that the WENSS 325 MHz flux density of all targets be greater than 500 mJy. This was done to ensure that strong optical depth limits could be achieved in relatively short GMRT integration times in this pilot project. A total of 24 AGNs, 6 at $3.0 < z < 3.6$ and 18 at $1.1 < z < 1.5$, were included in the pilot sample. We note, in passing, that there are only 2 AGNs from the CJF sample with searches for associated HI 21 cm absorption at $z \gtrsim 1$ in the literature (e.g. Gupta et al. 2006; Curran et al. 2013).

2.2 The GMRT observations and data analysis

The GMRT was used to observe the 24 CJF targets in November 2008 (proposal 15NKA01), with the 327 MHz and the 610 MHz receivers for sources at $3.0 < z < 3.6$ and $1.1 < z < 1.5$, respectively, and with the GMRT hardware correlator as the backend. The observations used bandwidths of 4 MHz (for the 327 MHz band) and 8 MHz (for the 610 MHz band), centred at the redshifted HI 21 cm line frequency of each target, and subdivided into 256 channels, using the high-resolution mode of the hardware correlator. This provided a total velocity coverage of $\approx 3200 - 3900 \text{ km s}^{-1}$ and a velocity resolution of $\approx 12 - 15 \text{ km s}^{-1}$. The typical on-source times were $\approx 1.0 \text{ hr}$ and $\approx 3 \text{ hrs}$ apiece, for sources observed with the 610 MHz and the 327 MHz bands, respectively. Observations of the standard flux calibrators 3C48, 3C147 or 3C286 were used to calibrate the GMRT's flux density scale, while (for most targets) nearby compact sources were used as secondary gain calibrators.

The initial GMRT searches yielded two absorption features, at $z = 1.198$ towards TXS 2356+390, and $z = 3.530$ towards TXS 0604+728. The first of these was a weak feature (with $\approx 5\sigma$ significance, after integrating over the profile), while the second had high ($\gtrsim 20\sigma$) significance. In addition, data on two targets (TXS 0707+476 and TXS 0014+813) were affected by RFI. We hence used the GMRT with its new software backend and 512 channels to re-observe all four systems in 2013 and 2014, using bandwidths of 4.17 MHz for TXS 0604+728 and 16.7 MHz for TXS 0014+813 (both observed with the 327 MHz band) and of

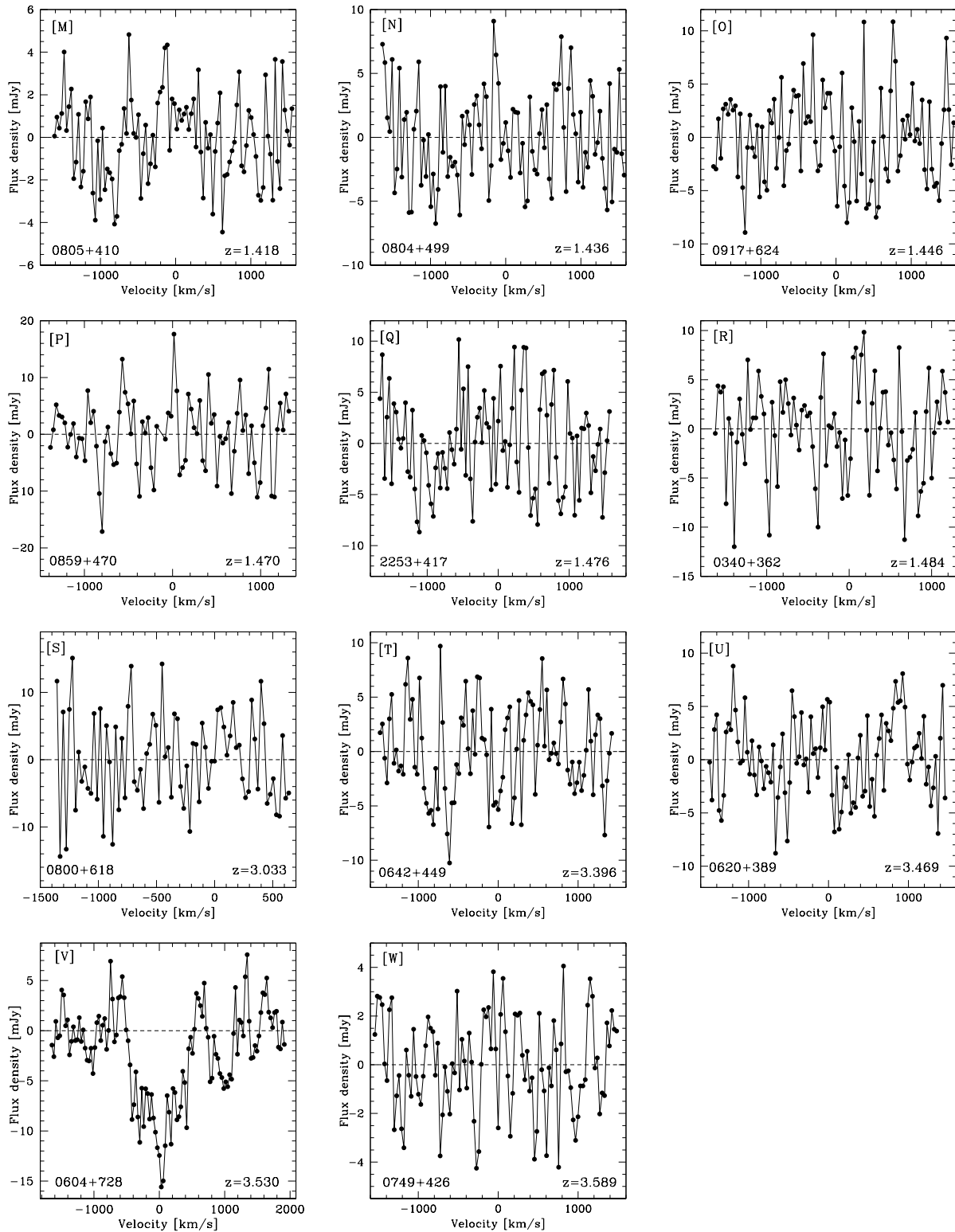


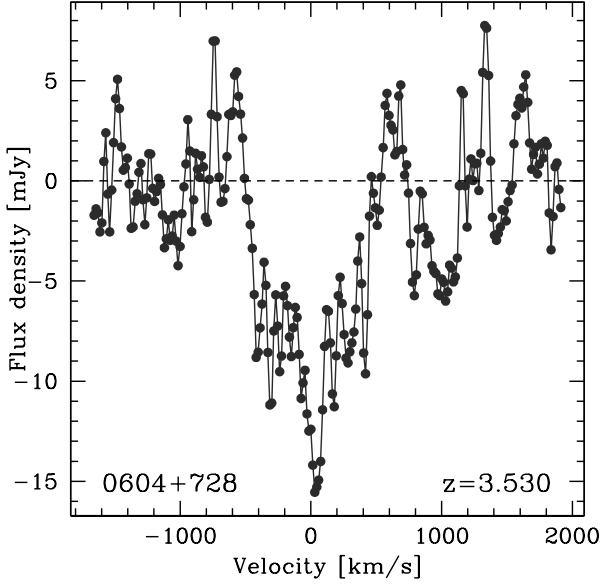
Figure 1. (contd.)

33.33 MHz for TXS 2356+390 and TXS 0707+476 (both observed with the 610 MHz band). The on-source times were again ≈ 1.0 hr (610 MHz band) and ≈ 3 hrs (327 MHz band) apiece.

All GMRT data were analysed in “classic” AIPS, using standard procedures. For each target source, the data were first carefully

inspected and edited to remove non-working antennas, bad correlator baselines, and time-specific problems, the latter usually arising due to intermittent radio frequency interference (RFI). Next, after calibration of the antenna-dependent gains and bandpass shapes, an iterative self-calibration procedure was followed for each target,

Figure 2. The GMRT HI 21 cm spectrum for the sole (tentative) detection of HI 21 cm absorption in our sample, at $z = 3.530$ towards TXS 0604+728. Note that the spectrum is at the original velocity resolution, i.e. it has not been Hanning-smoothed and re-sampled.



consisting of (typically) 3-4 rounds of phase-only self-calibration and imaging, followed by 1-2 rounds of amplitude-and-phase self-calibration and imaging, with additional data editing to remove corrupted data identified during the above process. This was carried out until the procedure converged to yield an image of the target that did not improve on further self-calibration. Since all our targets are unresolved at the GMRT angular resolution ($\approx 7''$ at 610 MHz and $\approx 12''$ at 327 MHz), the task JMFIT was then used to measure the flux density of each target via a single-Gaussian fit to a small region around the target source in the image plane. The continuum image was then subtracted from the calibrated U-V visibilities using the tasks UVSUB and UVLIN. Additional data editing was carried out at this stage, involving a detailed inspection of the residual dynamic spectra on all baselines. The residual U-V visibilities were then imaged to produce a “dirty” spectral cube, and a spectrum was obtained at the location of the target source via a cut through the cube. Finally, in some cases, a second-order polynomial was fit to each spectrum and subtracted out, to compensate for residual band-pass effects.

2.3 Results

The final GMRT HI 21 cm absorption spectra towards 23 of the 24 sources of the sample are shown in Fig. 1. Except for the tentative detection of HI 21 cm absorption towards TXS 0604+728, all spectra have been Hanning-smoothed and re-sampled. In the case of one source, TXS 0014+813, the GMRT data from multiple observing runs were affected by RFI and it was not possible to obtain a reliable RFI-free spectrum; this source will hence be excluded from the later discussion. For 21 sources, the GMRT spectra were consistent with noise, with no evidence for statistically significant absorption features. For two sources, TXS 2356+390 at $z = 1.198$ and TXS 0604+728 at $z = 3.530$, weak absorption features (with $\geq 5\sigma$ significance) were seen in the initial GMRT spectra. In the case of TXS 2356+390, the follow-up GMRT observations (with

somewhat worse sensitivity) ruled out the presence of HI 21 cm absorption at the level detected in the first observing run, indicating that the original feature is likely to have arisen due to low-level RFI. In the case of TXS 0604+728, at $z = 3.530$, the data from multiple GMRT observing runs following the original tentative detection were affected by strong RFI, and it was hence not possible to confirm or rule out the reality of the absorption feature. We note that the absorption feature towards TXS 0604+728 was detected via independent analysis procedures carried out by two of the authors, with independent data editing, and was also seen in the two independent polarizations, with consistent strengths. However, we can still not formally rule out the possibility that it arises from low-level RFI and hence will refer to it in the later discussion as a tentative detection. The final HI 21 cm spectrum towards TXS 0604+728 is also shown separately in Fig. 2 and the source is discussed in more detail below.

Table 1 summarizes the observational details and the results from the GMRT observations, with the sources ordered in increasing redshift. The columns of this table are (1) the source name, (2) the source redshift, (3) the observing frequency, $\nu_{21\text{ cm}}$, in MHz, (4) the observing bandwidth, BW, in MHz, (5) the velocity resolution Δv of the final spectra, in km s^{-1} (in all cases but one, TXS 0707+476, after Hanning-smoothing and re-sampling), (6) the source flux density, S_ν , measured using JMFIT, in mJy, (7) the RMS noise ΔS on the final spectrum at the velocity resolution listed in column (5), in mJy, (8) the integrated HI 21 cm optical depth τdV in km s^{-1} , or, for non-detections, the 3σ upper limit on $\int \tau dV$, assuming a line full-width-at-half maximum (FWHM) of 100 km s^{-1} , (9) the ultraviolet (UV) luminosity at a rest-frame wavelength of 1216 \AA of the AGN, (10) the rest-frame 1.4 GHz radio luminosity of the AGN, and (11) the low-frequency spectral index of the AGN, $\alpha_{21\text{ cm}}$, around the redshifted HI 21 cm line frequency. Note that the details provided for TXS 0707+476 are for the wide-band data set, with a bandwidth of 33.33 MHz and a velocity resolution of 31.5 km s^{-1} (without Hanning-smoothing and re-sampling).

For the non-detections, the limits on the integrated HI 21 cm optical depths were computed for an assumed line FWHM of 100 km s^{-1} , after smoothing the spectrum to a similar velocity resolution. Next, the luminosity at a rest-frame wavelength of 1216 \AA was estimated for each AGN following the prescription of Curran et al. (2008). For each AGN, we first determined the flux density F_{UV} at the wavelength $1216 \times (1+z) \text{ \AA}$ by interpolating between its measured flux densities in different optical and UV wavebands from the literature, fitting a power-law spectral shape. The luminosity at the rest-frame wavelength of 1216 \AA was then inferred from the expression $L_{UV} = 4\pi D_{AGN}^2 F_{UV}/(1+z)$. For two systems, TXS 0600+442 and TXS 2253+417, the luminosity is known only at a single optical waveband, quite distant from the redshifted 1216 \AA wavelength; these sources hence do not have a listed rest-frame 1216 \AA UV luminosity in the table. Finally, the radio spectral indices of the AGNs were computed from the flux densities at the redshifted HI 21 cm line frequency and the closest frequency with a flux density estimate (usually 1.4 GHz, from the Faint Images of the Radio Sky at Twenty-cm survey or the NRAO VLA Sky Survey (NVSS); Becker et al. 1995; Condon et al. 1998)

Figure 3. [A] Left panel: The integrated HI 21 cm optical depths of the 52 CJF sources of our full sample plotted versus redshift. The 23 sources whose HI 21 cm absorption spectra are presented in this paper are shown as squares, while the 29 literature sources are shown as triangles. Filled symbols indicate detections of HI 21 cm absorption, while open symbols indicate upper limits on the HI 21 cm optical depth. The dashed vertical line indicates the median redshift of the sample, $z_{\text{med}} = 0.76$. [B] Right panel: The detection rate of HI 21 cm absorption for the sub-samples with $z > z_{\text{med}}$ and $z < z_{\text{med}}$.

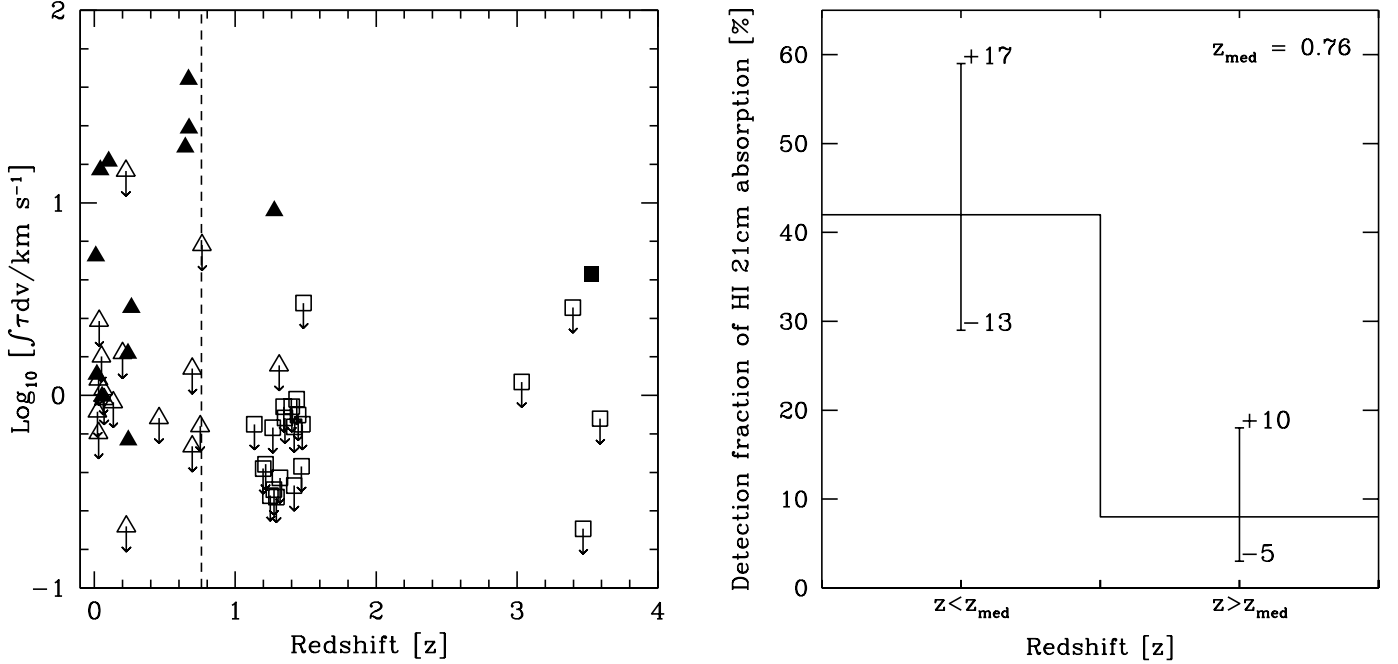


Figure 4. [A] Left panel: The rest-frame 1216 Å UV luminosity of 49 CJF sources of the sample plotted, in logarithmic units, versus the AGN redshift. The dotted horizontal line shows the median UV luminosity of the sample, $L_{\text{UV,med}} = 10^{22.0} \text{ W Hz}^{-1}$, while the dashed horizontal line shows the UV luminosity threshold of Curran et al. (2008) ($L_{\text{UV}} = 10^{23} \text{ W Hz}^{-1}$). [B] Right panel: The rest-frame 1.4 GHz radio luminosity $L_{1.4 \text{ GHz}}$ of the 52 CJF sources of the sample plotted, in logarithmic units, versus the AGN redshift. The dashed horizontal line shows the median rest-frame 1.4 GHz radio luminosity of the sample, $L_{1.4 \text{ GHz}} = 10^{27.3} \text{ W Hz}^{-1}$, while the dashed vertical line shows the median redshift of the sample, $z_{\text{med}} = 0.76$. The 23 sources of the present sample and the 29 literature systems are shown by squares and triangles, respectively, with filled and open symbols respectively indicating detections and non-detections of HI 21 cm absorption.

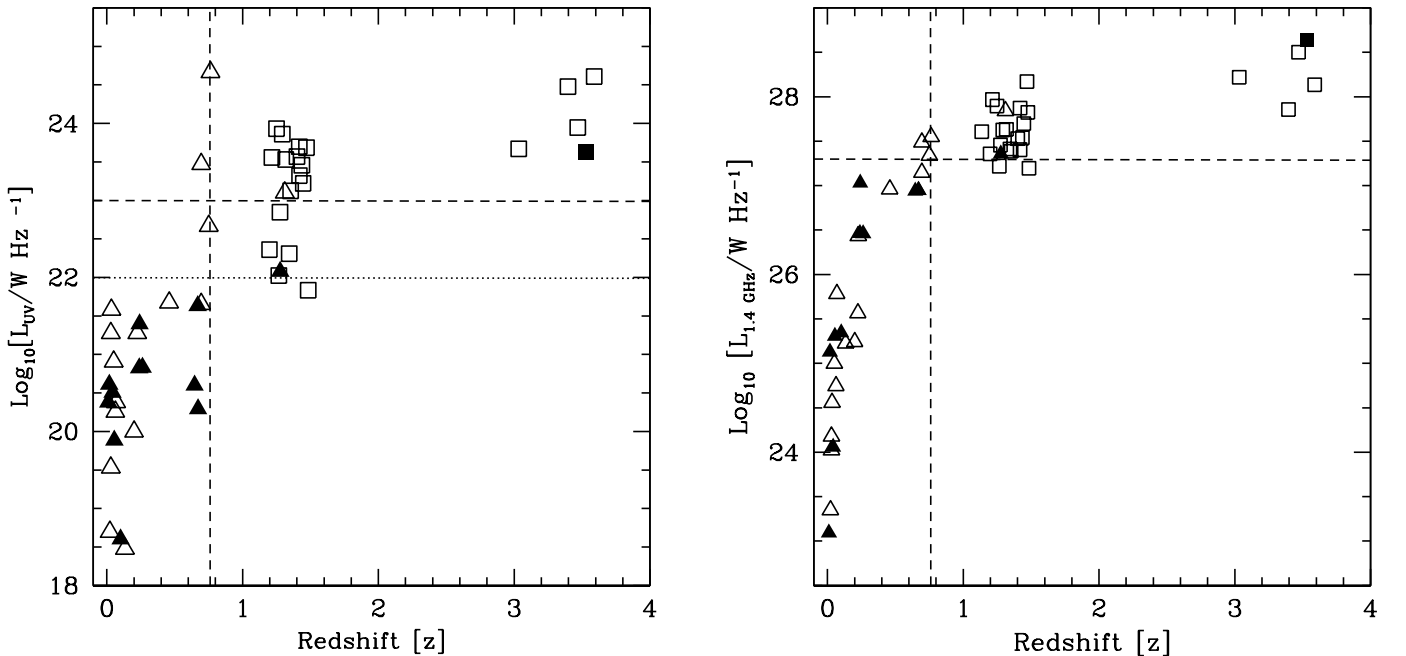


Figure 5. The integrated HI 21 cm optical depth plotted against [A] (Left panel) the rest-frame 1216 Å UV luminosity, and [B] (Right panel) the rest-frame 1.4 GHz radio luminosity, with all quantities in logarithmic units. Again, the 23 AGNs of this paper and the 29 literature sources are shown as squares and triangles, respectively, while filled and open symbols indicate detections of HI 21 cm absorption and upper limits on the HI 21 cm optical depth. The dashed vertical lines in the left and right panels indicate, respectively, the median rest-frame 1216 Å UV luminosity ($L_{UV,med} = 10^{22.0}$ W Hz⁻¹), and the median rest-frame 1.4 GHz radio luminosity ($L_{1.4\text{ GHz}} = 10^{27.3}$ W Hz⁻¹).

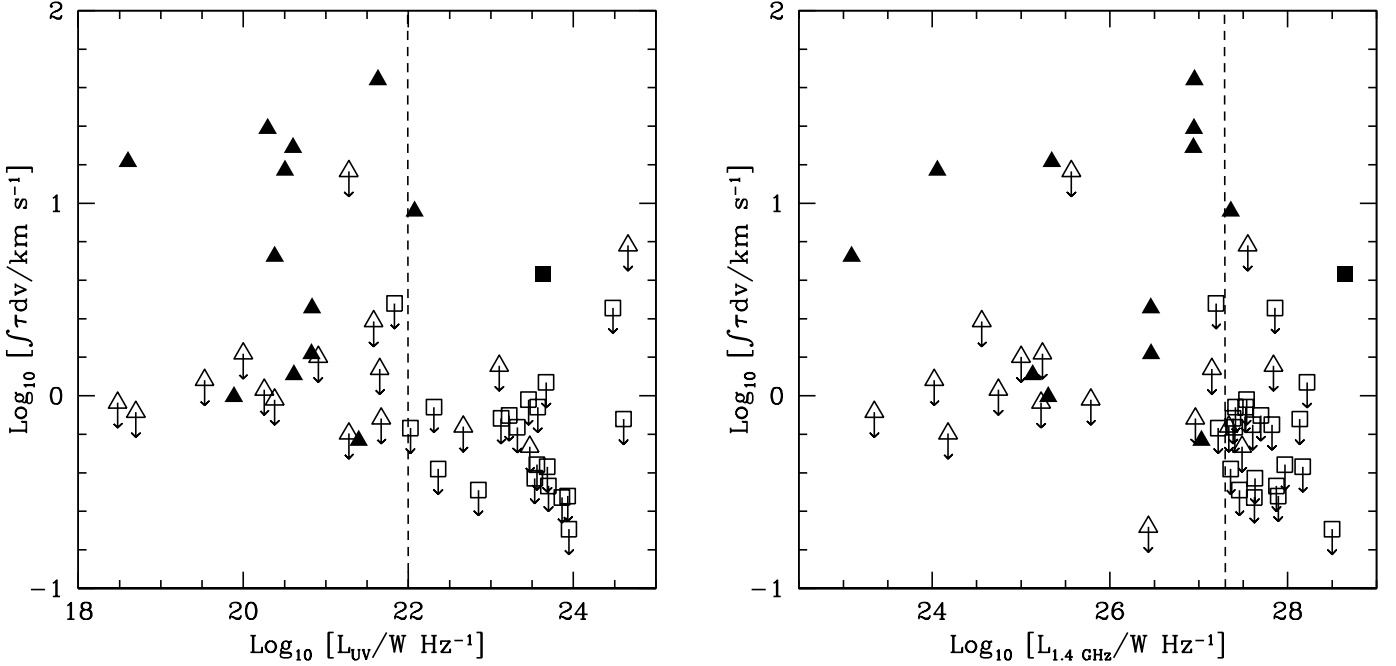
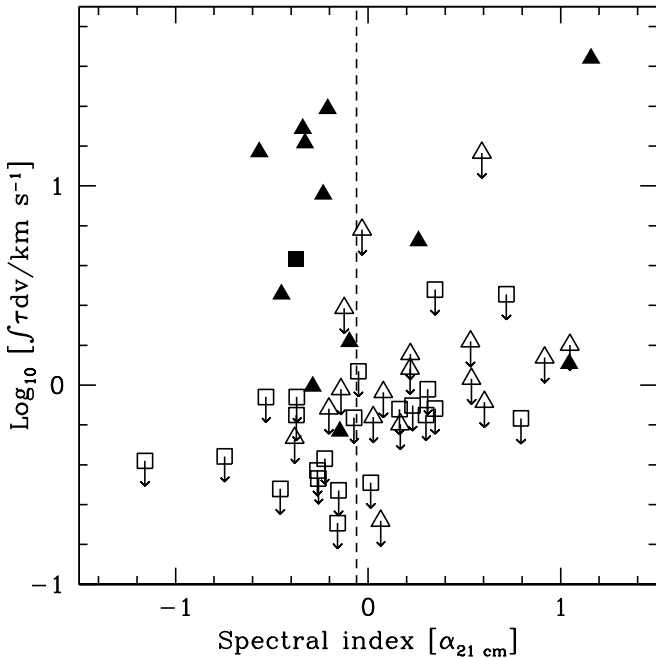


Figure 6. The integrated HI 21 cm optical depth plotted against the AGN low-frequency spectral index $\alpha_{21\text{ cm}}$, computed around the redshifted HI 21 cm line frequency. The 23 sources of this paper and the 29 literature sources are shown as squares and triangles, respectively, with filled and open symbols representing HI 21 cm detections and upper limits, respectively. The dashed vertical line indicates the median low-frequency spectral index of the sample, $\alpha_{21\text{ cm}, med} = -0.06$.



3 DISCUSSION

3.1 A uniformly-selected flat-spectrum sample

As noted in the introduction, there are only four known associated HI 21 cm absorbers at $z > 1$, corresponding to a low apparent detection rate of HI 21 cm absorption. However, there are more than 30 detections of HI 21 cm absorption at low redshifts, $z < 1$ (e.g. Vermeulen et al. 2003; Gupta et al. 2006; Geréb et al. 2015), with a typical reported detection fraction of $\gtrsim 30\%$ (e.g. Pihlström et al. 2003; Vermeulen et al. 2003). This suggests that the neutral gas content in the AGN environment (or physical conditions therein) may evolve with redshift. However, the comparison between the HI 21 cm detection fractions has mostly been carried out with heterogeneous AGN samples, where it is difficult to separate redshift evolution in the AGN environment from differences in the AGN samples at different redshifts. For example, Gupta et al. (2006) carried out a statistical analysis of 96 AGNs with associated HI 21 cm absorption studies, and found little evidence for redshift evolution in the detection rates of HI 21 cm absorption or the distribution of HI 21 cm optical depths. However, their sample was highly heterogeneous, consisting of 27 GPS sources, 35 compact steep spectrum sources, 13 flat-spectrum sources and 21 large radio galaxies; this makes it difficult to interpret their results.

An alternative explanation of a possible lower strength of HI 21 cm absorption in high- z AGNs arises from the fact that the high- z AGN sample typically contains objects of higher rest frame luminosities, in both the radio and the UV wavebands. Curran et al. (2008) noted that a high AGN luminosity in either of these bands might result in a lower strength of HI 21 cm absorption. Specifically, it has long been known that proximity to a strong radio source can alter the hyperfine level populations, increasing the gas

Table 2. The 29 CJF sources with HI 21 cm absorption searches in the literature, in order of increasing redshift. Note that $L'_{UV} = \text{Log}[L_{UV}/W \text{ Hz}^{-1}]$ and $L'_{1.4 \text{ GHz}} = \text{Log}[L_{1.4 \text{ GHz}}/W \text{ Hz}^{-1}]$.

Source	z	$\int \tau dV$ km s $^{-1}$	L'_{UV}	$L'_{1.4 \text{ GHz}}$	$\alpha_{21 \text{ cm}}$	Ref.
TXS 1146+596	0.0108	5.30	20.30	23.09	0.26	1
TXS 0316+413	0.0176	1.28	20.61	25.13	1.05	2
B3 0651+410	0.022	< 0.82	18.69	23.35	0.60	3
TXS 1101+384	0.030	< 0.63	21.28	24.18	0.17	4
TXS 1744+557	0.030	< 1.2	19.53	24.02	0.22	5
TXS 1652+398	0.034	< 2.4	21.58	24.56	-0.12	4
TXS 1254+571	0.042	14.8	20.51	24.06	-0.57	6
TXS 1807+698	0.051	< 1.6	20.91	25.00	1.05	4
TXS 0402+379	0.055	0.98	19.88	25.31	-0.29	7
TXS 1144+352	0.063	< 1.1	20.26	24.75	0.54	5
TXS 2200+420	0.069	< 0.95	20.30	25.78	-0.14	4
TXS 1946+708	0.101	16.46	18.60	25.35	-0.33	8
TXS 0309+411	0.134	< 0.92	18.48	25.23	0.08	5
IVS B1622+665	0.201	< 1.7	20.00	25.24	0.53	3
S5 1826+79	0.224	< 14.6	21.28	25.57	0.59	9
TXS 2021+614	0.227	< 0.21	—	26.43	0.07	9
TXS 2352+495	0.238	1.65	20.84	26.46	-0.09	9
TXS 0831+557	0.241	0.58	21.39	27.03	-0.15	9
TXS 1943+546	0.263	2.86	20.85	26.46	-0.45	9
TXS 1031+567	0.459	< 0.76	21.67	26.96	-0.20	9
TXS 1355+441	0.646	19.4	20.60	26.94	-0.34	9
S4 0108+38	0.669	43.77	21.63	26.95	1.16	10
TXS 1504+377	0.6715	24.4	20.30	26.95	-0.21	10
TXS 0923+392	0.695	< 0.54	23.47	27.49	-0.38	9
S5 0950+74	0.695	< 1.37	21.65	27.15	0.92	9
TXS 1642+690	0.751	< 0.69	22.66	27.34	0.03	9
S4 1843+35	0.764	< 6.0	24.66	27.55	-0.03	9
TXS 1543+480	1.277	9.1	22.08	27.36	-0.23	11
TXS 0248+430	1.311	< 1.4	23.10	27.84	0.22	1

References: (1) Gupta et al. 2006; (2) De Young et al. 1973; (3) Orienti et al. 2006; (4) van Gorkom et al. 1989; (5) Chandola et al. 2013; (6) Dickey 1982; (7) Morganti et al. 2009; (8) Peck et al. 1999; (9) Vermeulen et al. 2003; (10) Carilli et al. 1998; (11) Curran et al. 2013.

spin temperature, and thus lowering the HI 21 cm optical depth (Field 1959). Conversely, Curran et al. (2008) pointed out that a high AGN luminosity at UV wavelengths, $\lesssim 1216 \text{ \AA}$, might excite the electron in neutral hydrogen to higher energy levels (although this is unlikely to be an important effect, given the very short decay timescale to the ground state) or entirely ionize the gas, again lowering the strength of the HI 21 cm absorption. Both redshift evolution and dependence of local conditions on the AGN UV luminosity were found to be a viable explanations for the low observed strength of associated HI 21 cm absorption in high- z AGN (Curran et al. 2008, 2013). Again, however, their sample was highly heterogeneous, consisting of all radio sources in the literature with searches for associated HI 21 cm absorption.

Our targets have been selected from the CJF sample as flat-spectrum sources lying in the redshift ranges $1.1 < z < 1.5$ and $3.0 < z < 3.6$. A number of CJF sources, especially at lower redshifts $z < 0.7$, have HI 21 cm absorption studies in the literature (e.g. van Gorkom et al. 1989; Orienti et al. 2006; Gupta et al. 2006; Vermeulen et al. 2003; Curran et al. 2013). We have included these literature sources in our full sample in order to investigate the dependence of the HI 21 cm absorption strength on both redshift and AGN luminosity in a uniformly-selected sample. The literature sources are listed (ordered by increasing redshift) in Table 2, whose

columns are (1) the AGN name, (2) the AGN redshift, (3) the integrated HI 21 cm optical depth or, for HI 21 cm non-detections, the 3σ limit to the integrated HI 21 cm optical depth, in km s^{-1} (assuming a line FWHM of 100 km s^{-1}), (4) the AGN luminosity at a rest-frame wavelength of 1216 \AA (see Section 2.3 for details), (5) the AGN luminosity at a rest-frame frequency of 1.4 GHz, (6) the AGN spectral index around the redshifted HI 21 cm line frequency, $\alpha_{21 \text{ cm}}$, and (7) the literature reference to the HI 21 cm absorption study. There are 29 sources in the literature sample, with 12 detections of HI 21 cm absorption (11 at $z < 0.7$, and one at $z = 1.277$), and seventeen non-detections, sixteen of which are at $z < 0.8$. For one source, TXS 2021+6134, the luminosity is only known at a single optical waveband, far from the redshifted 1216 \AA wavelength; its rest-frame 1216 \AA UV luminosity is hence not listed in the table.

Our full sample thus consists of 52 sources selected from the CJF sample with associated HI 21 cm absorption studies, 23 from our observations and 29 from the literature, with 13 detections of HI 21 cm absorption (including our tentative detection towards TXS 0604+728) and 39 non-detections. This is the largest uniformly-selected sample of AGNs with redshifted HI 21 cm absorption studies; the median redshift of the sample is $z_{\text{med}} = 0.76$. In the following sections, we will examine the dependence of the

HI 21 cm detection fractions and the distribution of HI 21 cm optical depths on redshift, radio spectral index, and AGN radio and UV luminosity.

3.2 Redshift evolution

The left panel of Fig. 3 plots the integrated HI 21 cm optical depth (in logarithmic units) versus redshift for our full sample of 52 sources. The high sensitivity of our GMRT observations imply that the 3σ limits on the integrated HI 21 cm optical depths of our non-detections are in almost all cases (especially at redshifts $1.1 < z < 1.5$) sufficiently stringent to rule out HI 21 cm opacities comparable to those of the low- z detections of HI 21 cm absorption. It is clear from the figure that the detections of HI 21 cm absorption in this uniformly-selected flat-spectrum sample are concentrated in the redshift range $z < 0.7$, with only one detection at $z = 1.277$ (Curran et al. 2013), and a tentative detection at $z \approx 3.530$ (this work). On dividing the sample at the median redshift, $z_{\text{med}} = 0.76$, the low- z sample has 11 detections and 15 non-detections, i.e. a detection fraction of $42^{+17}_{-13}\%$, while the high- z sample has 2 detections (one of which is tentative) and 24 non-detections, for a detection fraction of $8^{+10}_{-5}\%$ (where the errors are from small-number Poisson statistics; e.g. Gehrels 1986). Thus, although the detection fraction appears to be higher at low redshifts, the difference in detection fractions in the high- z and low- z samples has only $\approx 2.1\sigma$ significance.

However, it also appears from Fig. 3[A] that the measured HI 21 cm optical depths for the low- z sample are higher than the typical upper limits to the HI 21 cm optical depths of the high- z sample. We hence used the Astronomical Survival analysis ASURV package (Isobe et al. 1986) to investigate whether there is indeed a difference in the distributions of the HI 21 cm optical depths of the low- z and high- z samples, taking into account the fact that some of the measurements are censored, i.e. are limits to the HI 21 cm optical depths. A Peto-Prentice generalized Wilcoxon two-sample test (for censored data) finds weak evidence that the HI 21 cm optical depths of the low- z and high- z samples are drawn from different distributions: the null hypothesis that they are drawn from the same sample is rejected at 2.7σ significance. Note that this result assumes the HI 21 cm absorption tentatively detected at $z = 3.530$ towards TXS 0604+728 is a real absorption feature. If this system (for which the HI 21 cm absorption remains to be confirmed) is excluded from the sample, the null hypothesis that the two samples are drawn from the same distribution is ruled out at $\approx 3.1\sigma$ significance in the Peto-Prentice test. While observations of a larger sample are needed to draw statistically reliable conclusions, we conclude that the present data show tentative evidence for redshift evolution in the strength of HI 21 cm absorption in AGN environments.

In passing, we note that, should the evidence for redshift evolution in the strength of associated HI 21 cm absorption be confirmed, this could imply either a lower typical HI column density or a lower cold gas fraction (i.e. a higher spin temperature) in the environments of high- z flat-spectrum AGNs. Unfortunately, this issue has often been ignored in studies of associated HI 21 cm absorption, where one does not have an independent estimate of the HI column density (unlike in the case of intervening HI 21 cm absorbers towards quasars, where one can usually determine the HI column density from the damped Lyman- α absorption line; e.g. Wolfe et al. 2005). Most associated HI 21 cm absorption studies in the literature assume a single spin temperature (usually, 100 or 1000 K) for the neutral gas in all AGNs and use this to convert the HI 21 cm optical

depth into an HI column density, and then discuss the evolution of the HI column density with redshift. We emphasize that it is very difficult to justify this assumption of a uniform spin temperature in AGN environments. Indeed, it is clear from HI 21 cm absorption studies of intervening damped Lyman- α systems (DLAs) that absorption-selected galaxies at high redshifts typically have high spin temperatures, indicating larger fractions of the warm neutral medium (e.g. Chengalur & Kanekar 2000; Kanekar & Chengalur 2003; Kanekar et al. 2014); this may well also be the case for AGN environments. It would hence be more appropriate in studies of associated HI 21 cm absorption to consider the dependence of the HI 21 cm optical depths, rather than the HI column density, on redshift, AGN luminosity, etc..

3.3 Dependence on the radio spectral index

A possible cause for the weakness of HI 21 cm absorption in the high- z AGN sample is that the radio emission of the high- z AGNs might be dominated by extended structure. While the targets have been chosen from the CJF sample, and are hence flat-spectrum sources (with $\alpha \geq -0.5$; Taylor et al. 1996), this spectral index is over the frequency range 1400 – 4850 MHz. At the lower frequencies of the redshifted HI 21 cm line, it is possible that the flat- or inverted-spectrum AGN core contributes a smaller fraction of the radio emission than the steep-spectrum extended structure. If so, the covering factor of neutral gas in the AGN environment could be low for high- z sources, thus reducing the apparent HI 21 cm optical depth. This might be tested by VLBI imaging of the radio continuum at or near the redshifted HI 21 cm line frequency (i.e. at frequencies < 1 GHz; e.g. Kanekar et al. 2009). Unfortunately, such low-frequency VLBI studies are not available for most of our target sources, especially the ones at high redshifts, $z > 1$. We will hence use the AGN spectral index *around the redshifted HI 21 cm line frequency* $\alpha_{21 \text{ cm}}$ as a proxy to estimate the compactness or lack thereof of the low-frequency radio emission: a flat spectrum would indicate core-dominated emission and a steep spectrum, extended structure. Fig. 6 plots the integrated HI 21 cm optical depth versus $\alpha_{21 \text{ cm}}$; the dashed vertical line indicates the median low-frequency spectral index, $\alpha_{21 \text{ cm, med}} = -0.06$. The figure shows that there are indeed a few sources with low-frequency spectral indices < -0.5 , i.e. steeper than the high-frequency spectral indices. However, we note that the median low-frequency spectral index remains close to 0, suggesting that the effect is not a strong one; indeed, there are only four sources with $\alpha_{21 \text{ cm}} < -0.5$. A Peto-Prentice two-sample test finds that the low- $\alpha_{21 \text{ cm}}$ and high- $\alpha_{21 \text{ cm}}$ sub-samples (separated at $\alpha_{21 \text{ cm, med}} = -0.06$) are consistent with being drawn from the same distribution (within 1.8σ significance). Excluding the tentative HI 21 cm detection towards TXS 0604+728 has only a marginal effect on the results: the sub-samples are then consistent with being drawn from the same distribution within 1.6σ significance. We conclude that there is no significant evidence that the apparent weakness in the HI 21 cm absorption in the high- z AGN sample arises due to the low-frequency radio emission being dominated by extended, steep-spectrum structure, and hence, a low AGN covering factor.

3.4 Dependence on the AGN luminosity

As noted above, the lower strength of HI 21 cm absorption in high-redshift AGNs could also arise if the high- z AGN sample is systematically biased towards objects with high UV or radio luminosities

(Curran et al. 2008). Fig. 4 tests this hypothesis by plotting (left panel) the rest-frame 1216 Å UV luminosities and (right panel) the rest-frame 1.4 GHz radio luminosities versus redshift (note that only 49 sources of the 52 are included in the left panel, as the remaining three do not have reliable estimates of their UV luminosity). It is apparent from the figure that AGNs of the high- z sample have significantly higher rest-frame 1216 Å UV and 1.4 GHz radio luminosities than those of the low- z sample. Again dividing the two samples at the median redshift $z_{\text{med}} = 0.76$, a Peto-Prentice two-sample test finds that the null hypothesis that the rest-frame UV luminosities of the two samples are drawn from the same distribution is ruled out at 6.4σ significance. Similarly, the null hypothesis that the rest-frame 1.4 GHz luminosities of the low- z and high- z samples are drawn from the same distribution is ruled out at 6.7σ significance. We conclude that our present flat-spectrum sample contains a strong bias towards higher rest-frame UV and 1.4 GHz luminosities at high redshifts. Similarly, the rest-frame UV and rest-frame 1.4 GHz luminosities are also strongly correlated for the sources of our sample.

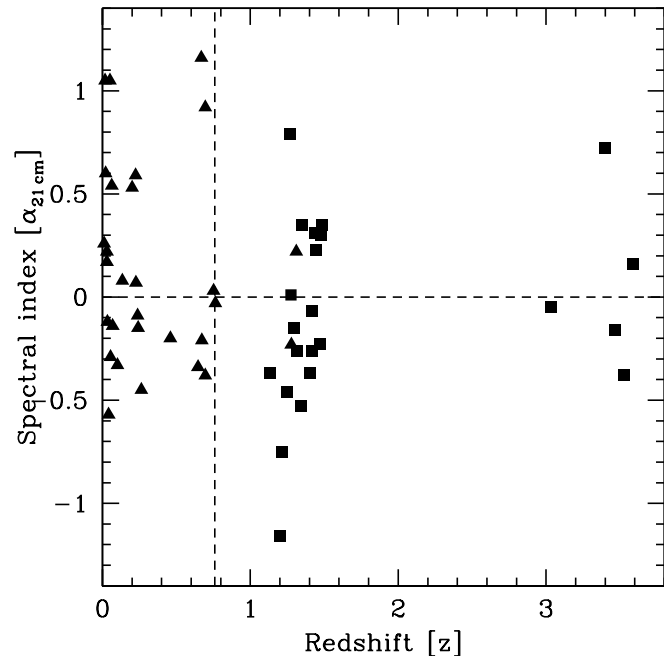
We hence considered the possibility that the apparent redshift evolution in the strength of the HI 21 cm absorption might arise due to the above luminosity bias. The two panels of Fig. 5 plot the integrated HI 21 cm optical depths (in logarithmic units) versus (left panel) the rest-frame 1216 Å UV luminosity, and (right panel) the rest-frame 1.4 GHz radio luminosity, both in logarithmic units. The median 1216 Å UV luminosity of our sample is $\text{Log}[L_{\text{UV,med}}/\text{WHz}^{-1}] = 22.0$, while the median 1.4 GHz luminosity of our sample is $\text{Log}[L_{1.4\text{ GHz,med}}/\text{WHz}^{-1}] = 27.3$. Dividing the low-luminosity and high-luminosity samples at the median luminosity for each case, a Peto-Prentice two-sample test finds that the hypothesis that the HI 21 cm optical depth distributions of the low- and high-luminosity samples are drawn from the same distribution is ruled out at 3.4σ significance for the rest-frame 1216 Å UV luminosity and at 3.1σ significance for the rest-frame 1.4 GHz radio luminosity. As above, if we exclude the tentative detection of HI 21 cm absorption towards TXS0604+728 from the sample, the above hypotheses are ruled out at 3.7σ and 3.4σ significance, respectively.

We thus find that the strength of the HI 21 cm absorption has a statistically significant dependence on redshift, rest-frame 1.4 GHz radio luminosity, and rest-frame 1216 Å UV luminosity, with weaker absorption being obtained at high redshifts and high AGN luminosities. Unfortunately, the luminosity bias in the sample, with the higher-luminosity AGNs located at higher redshifts, implies that the present sample does not allow us to distinguish between the three possibilities, and identify the primary cause, if any, of the decline in the strength of the HI 21 cm absorption in the high- z , high-luminosity sample. Observations of either a low-luminosity AGN sample at high redshifts or a high-luminosity AGN sample at low redshifts would be needed to break the degeneracy.

3.5 Covering factor issues

As mentioned earlier, there is no evidence that the non-detections of HI 21 cm absorption in the high- z CJF sample arise due to a low covering factor. However, a critical assumption in the interpretation of such associated HI 21 cm absorption studies, both in the present analysis and in the literature, is that the gas covering factor is unity for all systems, i.e. that the radio emission is entirely covered by any foreground gas. This is manifestly a poor assumption for certain classes of radio sources: for example, in Fanaroff-Riley-II galaxies, the radio emission is usually dominated by the large-

Figure 7. The AGN low-frequency spectral index $\alpha_{21\text{ cm}}$, computed around the redshifted HI 21 cm line frequency, plotted versus redshift. The 23 sources of this paper and the 29 literature sources are shown as squares and triangles, respectively. The dashed vertical line indicates the median redshift, $z = 0.76$.



scale lobes (e.g. O’Dea 1998). Even for compact steep spectrum sources, it is possible that the neutral gas lies close to the AGN core, and hence does not cover a significant fraction of the somewhat more extended steep spectrum source components. In this section, we hence consider the possibility that the AGN covering factor might be significantly different from unity, and its implications for our results.

First of all, it is clear that the results suggesting redshift evolution or AGN luminosity dependence are unchanged if *all* AGNs of the sample have low covering factors, provided the covering factors are the same. Further, the results of Section 3.2 suggest that the HI 21 cm absorption is stronger for low- z AGNs, even when the covering factor is assumed to be unity. If low- z AGNs have low covering factors, $f \ll 1$, we would have under-estimated the strength of their HI 21 cm absorption by assuming $f = 1$. In other words, a covering factor lower than unity for the low- z population can only increase the significance of the apparent redshift evolution. We hence consider three possibilities here, (1) AGNs at all redshifts have random covering factors, between 0 and unity, (2) low- z AGNs have high covering factors, ≈ 1 , while high- z AGNs have random covering factors, uniformly distributed between 0 and unity, and (3) low- z AGNs have high covering factors, $f \approx 1$, while high- z AGNs have low covering factors, $f \approx 0.1$.

For the first scenario, of all AGNs having random covering factors, the Peto-Prentice test finds that the null hypothesis that the low- z and high- z AGNs are drawn from the same population is rejected at $\approx 2.9\sigma$ and $\approx 3.2\sigma$ significance (depending, respectively, on whether we include or exclude the tentative detection of HI 21 cm absorption towards TXS 0604+728). These are very similar to the results on assuming a uniform covering factor of unity. Similarly, the null hypothesis that the low- and high-UV luminosity AGNs are drawn from the same distribution is re-

jected at $\approx 3.1\sigma$ (retaining TXS 0604+728) and $\approx 3.4\sigma$ (excluding TXS 0604+728) significance, while the hypothesis that the low- and high-radio luminosity AGNs are drawn from the same distribution is rejected at $\approx 3.0\sigma$ (retaining TXS 0604+728) and $\approx 3.3\sigma$ (excluding TXS 0604+728) significance. In other words, the results do not significantly change if one assumes that the AGNs of the sample have random covering factors, uniformly distributed between 0 and 1, instead of a single covering factor of unity.

For the second scenario, of the low- z AGNs having a covering factor of unity and the high- z ($z \geq 1$) AGNs having random covering factors, we find that the null hypotheses that the sub-samples are drawn from the same underlying distribution are rejected at $\approx 2.4\sigma$ and $\approx 2.7\sigma$ significance (with and without TXS 0604+728, respectively, for the low- z and high- z sub-samples), at $\approx 2.7\sigma$ and $\approx 3.1\sigma$ significance (with and without TXS 0604+728, respectively, for the low- and high-UV luminosity sub-samples), and at $\approx 2.6\sigma$ and $\approx 3.0\sigma$ significance (with and without TXS 0604+728, respectively, for the low- and high-radio luminosity sub-samples). While the statistical significances at which the null hypothesis is rejected are somewhat lower than in the case of unity covering factors, the results are again not significantly different.

Finally, in the third scenario, wherein low- z AGNs have a covering factor of unity and high- z ($z \geq 1$) AGNs have low covering factors ($f = 0.1$), we find that the null hypotheses that the sub-samples are drawn from the same distribution are rejected at far lower significance in all cases, $\approx 1.2\sigma$ and $\approx 1.7\sigma$ significance for the redshift sub-samples, $\approx 1.7\sigma$ and $\approx 2.2\sigma$ significance for the UV luminosity sub-samples, and $\approx 1.6\sigma$ and $\approx 2.1\sigma$ significance for the radio luminosity sub-samples (where, in all cases, the two values correspond to retaining and excluding TXS 0604+728). Thus, if high- z AGNs indeed have systematically lower covering factors than low- z systems, the present evidence for redshift evolution (or even for a luminosity dependence in the HI 21 cm absorption strength) is not statistically significant.

To test whether the high- z AGNs are indeed likely to have systematically lower covering factors than the low- z systems, we inspected the distribution of the radio spectral indices of the AGN sub-samples as a function of redshift. If the high- z AGNs have significantly steeper spectra at low frequencies, the radio emission of these systems is likely to arise from extended structure, rather than the core; if so, the high- z AGNs might have a systematically lower covering factor. Figure 7 plots the low-frequency radio spectral index ($\alpha_{21\text{ cm}}$) against redshift for our full sample of 52 AGNs; there is no obvious difference between the spectral indices of the low- and high- z sub-samples (separated by the dashed vertical line, at $z = 0.76$). A Gehan Wilcoxon two-sample test rules out the null hypothesis that the two sub-samples are drawn from the same distribution at $\approx 1.4\sigma$ significance, implying that the sub-samples are consistent with being drawn from the same distribution. Given that there appears to be no significant difference between their radio spectral indices, it appears unlikely that the high- z AGNs of our sample indeed have systematically lower covering factors than their low- z counterparts.

The results concerning the redshift and luminosity dependence of the strength of the HI 21 cm absorption thus appear to be robust if the covering factors are assumed to be random, either at all redshifts or only at high redshifts. It is only if the covering factors are assumed to be high for low- z AGNs and systematically low for high- z AGNs that the null hypothesis that the sub-samples are drawn from the same population cannot be ruled out at high (i.e. $\approx 3\sigma$) significance. This scenario appears unlikely, as the high- z and low- z AGN samples have similar spectral index distributions.

We hence conclude that our results do not appear to strongly depend on the assumption that the AGN covering factor is unity.

3.6 The HI 21 cm absorber at $z = 3.530$ towards TXS 0604+728

If confirmed, the absorption feature towards TXS 0604+728 would be at the highest redshift at which HI 21 cm absorption has ever been discovered, surpassing the two absorbers at $z \approx 3.39$ towards TXS 0902+343 (Uson et al. 1991) and PKS 0201+113 (Kanekar et al. 2007). The putative HI 21 cm absorption is extremely wide, with a full width between 20% points of $\approx 850\text{ km s}^{-1}$. For comparison, the associated HI 21 cm absorbers in the samples of Geréb et al. (2015) or Vermeulen et al. (2003) all have velocity widths (between 20% points) $\leq 825\text{ km s}^{-1}$. The absorption appears symmetric about the source redshift, but the signal-to-noise ratio of the present spectrum is not sufficient to derive detailed kinematic information.

TXS 0604+728 has a complicated core-jet structure on angular scales ranging from milli-arcsecs to ≈ 10 arcsecs (e.g. Taylor et al. 1994, 1996; Britzen et al. 2007). It has a spectral index of $\alpha = -0.35$ ($S_\nu \propto \nu^\alpha$) between 1.4 GHz and 4.8 GHz (Taylor et al. 1996), steepening slightly to $\alpha \approx -0.44$ between 325 GHz and 1.4 GHz (using 1420 MHz and 327 MHz flux densities from the NVSS and the Westerbork Northern Sky Survey, respectively; Condon et al. 1998; Rengelink et al. 1997). The wide absorption profile could arise due to absorption against different radio source components in the core and the jets.

Finally, TXS 0604+728 has a high estimated UV luminosity, $\approx 4.2 \times 10^{23}\text{ W Hz}^{-1}$, using a template to extrapolate from the measured luminosities in optical wavebands. If the reality of the absorption feature of Fig. 2 is confirmed, it would be the first case of a detection of HI 21 cm absorption in an AGN with UV luminosity $\gtrsim 10^{23}\text{ W Hz}^{-1}$. This UV luminosity has been suggested as the threshold above which the HI in the AGN environment is either ionized or excited to higher energy states (see discussion below; Curran et al. 2011); the latter authors argue that HI absorption should hence not be detectable in AGNs with UV luminosities above this threshold. While there is little evidence in support of this argument (as discussed above, the lack of HI 21 cm absorption in present high- z , high-luminosity samples may arise either from redshift evolution, or due to a UV or a radio luminosity threshold, to mention just three possibilities), it also only applies to HI in the vicinity of the AGN. In the case of AGNs with extended radio continuum, such as TXS 0604+728, more distant neutral gas could well give rise to HI 21 cm absorption.

4 SUMMARY

In summary, we have used the GMRT to carry out a search for redshifted HI 21 cm absorption from neutral gas associated with 24 flat-spectrum AGNs, at redshifts $1.1 < z < 1.5$ and $3.0 < z < 3.6$, and selected from the Caltech-Jodrell Flat-spectrum sample. We obtained a single tentative detection of HI 21 cm absorption, at $z = 3.530$ towards TXS 0604+728, and 22 non-detections of HI 21 cm absorption, with stringent constraints on the HI 21 cm optical depth; the data on the last target was not usable due to RFI. Including data from the literature, 52 CJF sources have now been searched for associated HI 21 cm absorption, with a median sample redshift of $z_{\text{med}} = 0.76$. We used two-sample tests to find $\approx 3\sigma$ evidence that the HI 21 cm absorption is stronger at low

redshifts, and towards AGNs with low UV/radio luminosities. The results are robust to different assumed covering factors, except for the case that the AGN covering factors are assumed to be systematically low in the high-*z* sub-sample. Using the radio spectral index as a measure of the AGN compactness, we find no evidence that the high-*z* AGNs are systematically less compact than the low-*z* AGNs; it hence appears unlikely that the high-*z* AGN sub-sample indeed have systematically and significantly lower covering factors than the low-*z* sub-sample. This is the first time that statistically significant evidence has been obtained for a redshift or luminosity dependence of the strength of HI 21 cm absorption in a uniformly selected sample. Unfortunately, the luminosity bias of the sample, with high-luminosity systems predominantly arising at high redshifts, implies that it is currently not possible to separate redshift evolution and AGN luminosity as the causes for the weakness of the HI 21 cm absorption in high-*z*, high-luminosity active galactic nuclei.

ACKNOWLEDGEMENTS

We thank Jayaram N. Chengalur for comments on an earlier version of this paper. We also thank the staff of the GMRT who have made these observations possible. The GMRT is run by the National Centre for Radio Astrophysics of the Tata Institute of Fundamental Research. SK and NK acknowledge support from, respectively, the NCRA-TIFR Visiting Students' Research Programme and the Department of Science and Technology through a Swarnajayanti Fellowship (DST/SJF/PSA-01/2012-13).

REFERENCES

Allen S. W., Dunn R. J. H., Fabian A. C., Taylor G. B., Reynolds C. S., 2006, *MNRAS*, 372, 21
 Barthel P. D., 1989, *ApJ*, 336, 606
 Becker R. H., White R. L., Helfand D. J., 1995, *ApJ*, 450, 559
 Britzen S. et al., 2007, *A&A*, 472, 763
 Carilli C. L., Menten K. M., Reid M. J., Rupen M. P., 1997, *ApJ*, 474, L89
 Carilli C. L., Menten K. M., Reid M. J., Rupen M. P., Yun M. S., 1998, *ApJ*, 494, 175
 Carilli C. L. et al., 2000, *Phys. Rev. Lett.*, 85, 5511
 Carilli C. L., Perlman E. S., Stocke J. T., 1992, *ApJ*, 400, L13
 Carilli C. L., Wrobel J. M., Ulvestad J. S., 1998, *AJ*, 115, 928
 Chandola Y., Gupta N., Saikia D. J., 2013, *MNRAS*, 429, 2380
 Chengalur J. N., Kanekar N., 2000, *MNRAS*, 318, 303
 Chengalur J. N., Kanekar N., 2003, *Phys. Rev. Lett.*, 91, 241302
 Condon J. J., Cotton W. D., Greisen E. W., Yin Q. F., Perley R. A., Taylor G. B., Broderick J. J., 1998, *AJ*, 115, 1693
 Conway J. E., Blanco P. R., 1995, *ApJ*, 449, L131
 Curran S. J. et al., 2011, *MNRAS*, 413, 1165
 Curran S. J., Whiting M. T., Sadler E. M., Bignell C., 2013, *MNRAS*, 428, 2053
 Curran S. J., Whiting M. T., Wiklind T., Webb J. K., Murphy M. T., Purcell C. R., 2008, *MNRAS*, 391, 765
 De Young D. S., Roberts M. S., Saslaw W. C., 1973, *ApJ*, 185, 809
 Dickey J. M., 1982, *ApJ*, 263, 87
 Douglas J. N., Bash F. N., Bozyan F. A., Torrence G. W., Wolfe C., 1996, *AJ*, 111, 1945

Drinkwater M. J., Webb J. K., Barrow J. D., Flambaum V. V., 1998, *MNRAS*, 295, 457
 Efstathiou G., 2000, *MNRAS*, 317, 697
 Fabian A. C., 2012, *ARA&A*, 50, 455
 Field G. B., 1959, *ApJ*, 129, 536
 Gehrels N., 1986, *ApJ*, 303, 336
 Geréb K., Maccagni F. M., Morganti R., Oosterloo T. A., 2015, *A&A*, 575, 44
 Gupta N., Salter C. J., Saikia D. J., Ghosh T., Jeyakumar S., 2006, *MNRAS*, 373, 972
 Henstock D. R., Browne I. W. A., Wilkinson P. N., McMahon R. G., 1997, *MNRAS*, 290, 380
 Henstock D. R., Browne I. W. A., Wilkinson P. N., Taylor G. B., Vermeulen R. C., Pearson T. J., Readhead A. C. S., 1995, *ApJS*, 100, 1
 Ishwara-Chandra C. H., Dwarakanath K. S., Anantharamaiah K. R., 2003, *JA&A*, 24, 37
 Isobe T., Feigelson E. D., Nelson P. I., 1986, *ApJ*, 306, 490
 Kanekar N., Briggs F. H., 2004, *New Astr. Rev.*, 48, 1259
 Kanekar N., Chengalur J. N., 2002, *A&A*, 381, L73
 Kanekar N., Chengalur J. N., 2003, *A&A*, 399, 857
 Kanekar N., Chengalur J. N., 2008, *MNRAS*, 384, L6
 Kanekar N., Chengalur J. N., Ghosh T., 2004, *Phys. Rev. Lett.*, 93, 051302
 Kanekar N., Chengalur J. N., Ghosh T., 2010, *ApJ*, 716, L23
 Kanekar N., Chengalur J. N., Lane W. M., 2007, *MNRAS*, 375, 1528
 Kanekar N., Lane W. M., Momjian E., Briggs F. H., Chengalur J. N., 2009, *MNRAS*, 394, L61
 Kanekar N. et al., 2014, *MNRAS*, 438, 2131
 Moore C. B., Carilli C. L., Menten K. M., 1999, *ApJ*, 510, L87
 Morganti R., 2012, *Using HI Absorption to Trace Outflows from Galaxies and Feeding of AGN*. Springer-Verlag Berlin Heidelberg, p. 31
 Morganti R., Fogasy J., Paragi Z., Oosterloo T., Orienti M., 2013, *Science*, 341, 1082
 Morganti R., Oosterloo T., Struve C., Saripalli L., 2008, *A&A*, 485, L5
 Morganti R., Oosterloo T. A., Tadhunter C. N., van Moorsel G., Killeen N., Wills K. A., 2001, *MNRAS*, 323, 331
 Morganti R., Peck A. B., Oosterloo T. A., van Moorsel G., Capetti A., Fanti R., Parma P., de Ruiter H. R., 2009, *A&A*, 505, 559
 O'Dea C. P., 1998, *PASP*, 110, 493
 Orienti M., Morganti R., Dallacasa D., 2006, *A&A*, 457, 531
 Pearson T. J., Readhead A. C. S., 1988, *ApJ*, 328, 114
 Peck A. B., Taylor G. B., 2002, *New Astr. Rev.*, 46, 273
 Peck A. B., Taylor G. B., Conway J. E., 1999, *ApJ*, 521, 103
 Pihlström Y. M., Conway J. E., Vermeulen R. C., 2003, *A&A*, 404, 871
 Polatidis A. G., Wilkinson P. N., Xu W., Readhead A. C. S., Pearson T. J., Taylor G. B., Vermeulen R. C., 1995, *ApJS*, 98, 1
 Rees M. J., 1984, *ARA&A*, 22, 471
 Rengelink R. B., Tang Y., de Bruyn A. G., Miley G. K., Bremer M. N., Röttgering H. J. A., Bremer M. A. R., 1997, *A&AS*, 124, 259
 Springel V., Di Matteo T., Hernquist L., 2005, *MNRAS*, 361, 776
 Struve C., Oosterloo T. A., Morganti R., Saripalli L., 2010, *A&A*, 515, A67
 Taylor G. B., Vermeulen R. C., Pearson T. J., Readhead A. C. S., Henstock D. R., Browne I. W. A., Wilkinson P. N., 1994, *ApJS*, 95, 345
 Taylor G. B., Vermeulen R. C., Readhead A. C. S., Pearson T. J.,

- Henstock D. R., Wilkinson P. N., 1996, *ApJS*, 107, 37
Uson J. M., Bagri D. S., Cornwell T. J., 1991, *Phys. Rev. Lett.*,
67, 3328
van Gorkom J. H., Knapp G. R., Ekers R. D., Ekers D. D., Laing
R. A., Polk K. S., 1989, *AJ*, 97, 708
Vermeulen R. C. et al., 2003, *A&A*, 404, 861
Wiklind T., Combes F., 1994, *A&A*, 286, L9
Wiklind T., Combes F., 1996, *A&A*, 315, 86
Wolfe A. M., Gawiser E., Prochaska J. X., 2005, *ARA&A*, 43,
861